Applied Science and Engineering Progress, Vol. 20, No. 4, 2027, 8321

Research Article

Phytogenic Selenium Nanoparticles from *Gracilaria vermiculophylla* Byproduct: Synthesis and Characterization

Dzikri Wahyudi
Faculty of Fisheries and Marine Sciences, Brawijaya University, Malang, Indonesia; and Marine and Fisheries Polytechnic, Karawang, Indonesia

Uun Yanuhar*, Andi Kurniawan and Nico Rahman Caesar
Study Program of Aquatic Resource Management, Faculty of Fisheries and Marine Sciences, Brawijaya University, Malang, Indonesia

Abdul Rahem Faqih
Study Program of Aquaculture, Faculty of Fisheries and Marine Sciences, Brawijaya University, Malang, Indonesia

Heru Suryanto
Department of Mechanical and Industrial Engineering, Faculty of Engineering, State University of Malang, Malang, Indonesia

Defa Rizqi Machfuda
Faculty of Fisheries and Marine Sciences, Brawijaya University, Malang, Indonesia

* Corresponding author. E-mail: doktoruun@ub.ac.id DOI: 10.14416/j.asep.2026.09.014
Received: 6 July 2026; Revised: 15 August 2026; Accepted: 24 August 2026; Published online: 23 September 2026

Abstract
Selenium (Se) is an essential trace element involved in antioxidant defense, immune regulation, and physiological processes in aquatic organisms; however, conventional inorganic Se supplementation has limited safety margins. This study developed phytogenic selenium nanoparticles (SeNPs) using sodium selenite (Na_2SeO_3) and extract derived from *Gracilaria vermiculophylla* processing byproducts as a natural reducing and stabilizing agent. The physicochemical properties of SeNPs were characterized using UV-Vis spectroscopy, Fourier transform infrared spectroscopy (FTIR), particle size analysis (PSA), field-emission scanning electron microscopy (FESEM), energy dispersive X-ray spectroscopy (EDS), and X-ray diffraction (XRD). Biological toxicity was evaluated using the rotifer, *Brachionus plicatilis*. Liquid chromatography coupled with high resolution mass spectrometry (LC-HRMS) profiling revealed putative phenolic, terpenoid, and steroid-like metabolites potentially involved in SeNP formation. The optimal synthesis condition occurred at 30 °C, producing brick-red colloids with a characteristic absorption peak at 320-330 nm. The synthesized SeNPs exhibited spherical morphology, an average particle size of approximately 50 nm, and a hexagonal selenium crystalline structure. Acute toxicity increased with exposure duration, reaching 22.22-57.78% mortality after 48 h with an LC_{50} value of 3.76 mg L^{-1}. CLSM confirmed SeNP localization mainly in the digestive and internal regions of *B. plicatilis*. These findings demonstrate the feasibility of *G. vermiculophylla*-derived SeNPs as a sustainable selenium source for further aquaculture applications.

Keywords: Acute toxicity, *Brachionus plicatilis*, *Gracilaria vermiculophylla*, Phytogenic synthesis, Selenium nanoparticles

Applied Science and Engineering Progress, Vol. 20, No. 4, 2027, 8321

1 Introduction

The rapid expansion of the seaweed cultivation and processing industry has produced large amounts of residual biomass that has not been utilized optimally, even though this biomass contains valuable bioactive compounds. Previous studies showed that processing residues of *Gracilaria sp*. have an estimated potential of 52 metric tons per year from biomass waste [1]. Indonesia is one of the world's largest seaweed-producing countries, with annual production exceeding 9.2 million tons, resulting in considerable biomass residues from harvesting and processing activities [2]. In the processing sequence for *Gracilaria* spp., which includes sorting, drying, pressing, and product preparation, by-products are generally discarded [3]. These materials may retain functional biomolecules, such as polysaccharides, proteins, phenolic compounds, pigments, and other secondary metabolites [4]. By reducing biomass waste and generating sustainable sources for biotechnological applications, the conversion of seaweed processing residues into value-added functional materials represents an important strategy within circular bioeconomy strategies [5].

Selenium (Se) is a crucial trace element that enters the body via selenoproteins, playing a role in redox control, immunological modulation, antioxidant defense, thyroid hormone metabolism, and physiological development in aquatic species [4]. Se supplements are used in aquaculture to improve physiological resilience and nutritional condition. Inorganic Se sources such as sodium selenite exhibit several drawbacks, including oxidative instability, a narrow margin between beneficial and toxic dosages, fluctuating bioavailability, and potential environmental issues [6].

These limitations underscore the need for alternative selenium delivery methods that offer greater effectiveness and improved biological compatibility. Because of their enormous surface area, adjustable surface properties, and nanoscale dimensions, SeNPs have been identified as a viable selenium delivery mechanism [6]. According to earlier studies, if the dosage and exposure conditions are suitable, SeNP supplementation can improve growth performance, immune related indicators, and antioxidant responses in a variety of aquaculture species [7]. However, the size of the nanoparticles, surface chemistry, aggregation behavior, length of exposure, and species-specific reactions all have a major impact on these biological consequences [8].

Understanding the physicochemical characteristics of SeNPs and their biological interactions as useful selenium delivery agents is necessary for broader use in aquaculture systems. Fresh plant extracts, pure biomolecules, or traditional biological sources are of great interest in green synthesis, or ecologically friendly synthesis [8]. Particularly with regard to the connections between extract-derived metabolites, SeNPs physicochemical properties, and biosafety responses, the potential of seaweed processing by-products as sustainable sources of reducing and surface-associated biomolecules is yet mainly unexplored [9]. Therefore, it is essential to comprehend how metabolites formed from byproducts affect the creation of nanoparticles and biological performance in order to advance circular biobased nanotechnology [10]. Their abundance and varied chemical composition, which includes proteins, pigments, polysaccharides, and phenolic compounds, make macroalga extracts excellent biological platforms for SeNPs production [11].

The marine rotifer *Brachionus plicatilis* represents an important biological model for evaluating nanoparticle interactions in aquaculture because of its ecological relevance, short life cycle, sensitivity to environmental stressors, and extensive use as live feed for marine fish larvae [12]. Beyond its role as a nutritional organism, *B. plicatilis* can function as a biological nutrient carrier capable of accumulating and potentially delivering enriched nutrients to early stage fish larvae [13]. Previous studies have investigated nanoparticle toxicity in rotifers using materials such as Ag, ZnO, Fe_3O_4 and TiO_2 nanoparticles [14]-[17]. However, information regarding the biological responses of rotifers exposed to phytogenic SeNPs remains limited. In particular, the influence of SeNP synthesis conditions and resulting physicochemical characteristics on acute toxicity responses and fluorescence associated distribution patterns in *B. plicatilis* has not been fully elucidated [18]. Physicochemical characterization alone cannot predict biological responses, whereas toxicity assessment without nanoparticle characterization provides limited interpretation of nanoparticle biological interactions and potential application for aquaculture.

Accordingly, this study hypothesized that bioactive compounds present in *Gracilaria vermiculophylla* processing byproducts facilitate phytogenic SeNP formation and influence the physicochemical properties and biological responses of the resulting nanoparticles. This study aimed to synthesize SeNPs using *G. vermiculophylla* processing

Applied Science and Engineering Progress, Vol. 20, No. 4, 2027, 8321

byproduct extract and characterize the physicochemical properties and their toxicity against the marine rotifer *B. plicatilis*.

2 Materials and Methods

2.1 *Materials*

Gracilaria seaweed processing by-products were collected from a seaweed processing facility in Karawang, Indonesia. The marine rotifer *Brachionus plicatilis,* and sodium selenite (Na_2SeO_3, 99% purity; Sigma Aldrich) were used as a selenium precursor in the synthesis of SeNPs. 99% ethanol, 37% hydrochloric acid (HCl), 1 N sodium hydroxide solution (NaOH), and distilled water were used for extraction, synthesis, washing, and sample preparation. All reagents were of analytical grade. For fluorescence tracking, SeNPs were labeled with Rhodamine B suitable for fluorescence (Sigma Aldrich).

2.2 *Methods*

2.2.1 Collection and mechanical sorting of G. vermiculophylla by-products

G. vermiculophylla by-products are collected during the initial mechanical cleaning stage of seaweed processing. The collected biomass consists of small seaweed fragments separated from commercial raw materials. The mechanically sorted biomass is then collected as a raw material for extract production and phytogenic SeNP synthesis.

2.2.2 Extraction of Gracilaria vermiculophylla by-product

G. vermiculophylla by-products (2 Kg) were dried at 50°C for 2 hours to remove humidity. Dried biomass was ground into a fine powder. 10 g of dried biomass powder was diluted with 100 mL of absolute ethanol (1:10, w/v). The UCD-950 ultrasonic processor (Biobase, China) was used to assist in the extraction with a power rate setting of 50% for 20 minutes with a 5-second pulse interval, a frequency of 20 kHz, and a temperature maintained below 40°C. The extract was filtered using Whatman No. 1 filter paper and concentrated using a rotary vacuum evaporator. The obtained extract was stored at -20°C until further analysis [10].

2.2.3 LC-HRMS-based metabolite profiling

LC-HRMS analysis was performed to characterize putative metabolites present in the *G. vermiculophylla* byproduct extract. Analysis was conducted using a Dionex Ultimate 3000 RSLC nano system coupled with a Q Exactive Orbitrap high-resolution mass spectrometer (Thermo Fisher Scientific, USA). Chromatographic separation was performed using an Accucore C18 column (50 × 2.1 mm, 2.6 µm particle size) with a mobile phase consisting of LC-MS grade water containing 0.1% formic acid (A) and acetonitrile containing 0.1% formic acid (B). Gradient elution was carried out at a flow rate of 0.2 mL min^{-1}, with the proportion of phase B ranging from 5% to 95% over 30 minutes. Metabolite annotation was based on accurate mass, retention time, and database matching.

2.2.4 Phytogenic synthesis of SeNPs

A modified method for the phytogenic synthesis of SeNPs was developed based on previous techniques [19], [20]. Sodium selenite (Na_2SeO_3) was used as the selenium precursor for the phytogenic production of SeNPs. Briefly, a Na_2SeO_3 solution (20 mM) prepared with distilled water was mixed with 5 mL of *G. vermiculophylla* by-product extract. A magnetic stirrer was used to continuously stir the reaction mixture at 400 rpm until the final volume reached 50 mL. To assess the effect of temperature on SeNPs production and physicochemical properties, nanoparticle synthesis was conducted at three different temperatures (30°C, 35°C, and 45°C). The observed color change from greenish-brown to brick red indicated that the reaction was proceeding. Following synthesis, the colloidal suspension was centrifuged at 12,000 rpm for 15 minutes to remove residual extract components. The resulting SeNP suspension was stored at 4°C prior to physicochemical characterization.

2.2.5 Nanoparticle characterization

To analyze the optical characteristics, chemical structure, and constituent components of the selenium nanoparticles, this study employed various analytical instruments as follows.

UV-Vis spectrophotometer

The optical characteristics of the produced SeNPs were evaluated using a UV-Vis spectrophotometer (Shimadzu, Japan). Prior to analysis, the SeNP

Applied Science and Engineering Progress, Vol. 20, No. 4, 2027, 8321

colloidal suspension was gently homogenized, and 1 mL of each sample was transferred into a quartz cuvette (1 cm optical path length), using pure water as a blank reference. Absorption spectra were observed within the 200 to 700 nm wavelength range at room temperature. The formation and optical behavior of the phytogenic SeNPs were assessed based on changes in absorption intensity, the wavelength of maximum absorption (λmax), and spectral broadening associated with nanoparticle synthesis, dispersion characteristics, and aggregation potential. The UV-Vis data were interpreted with the aid of various supplementary analyses, including FESEM, PSA, FTIR, and XRD.

Functional group analysis

Functional groups involved in SeNP synthesis and surface stability were investigated using Fourier-transform infrared (FTIR) spectroscopy (Shimadzu, Japan). The SeNP suspension was centrifuged for 15 minutes at 4 °C and 12,000 rpm, washed twice with ultrapure water, and then resuspended to form a concentrated colloid. A 20 µL aliquot was placed directly onto the ATR crystal to record spectra in the 4000-400 cm^{-1} range, using 50 scans at a resolution of 8 cm^{-1} after subtracting the water background. The obtained spectra were evaluated based on characteristic absorption bands associated with hydroxyl, carbonyl, amide, and carboxylate groups following baseline correction.

Particle size analysis (PSA)

Particle size analysis using the laser diffraction method (SALD-7500nano, Shimadzu, Japan) was performed to determine the size distribution of the produced SeNPs. For sample preparation, ultrapure water was added to a 1.0 mL aliquot of the initial SeNP colloidal suspension, resulting in a tenfold dilution to a final volume of 10.0 mL. To enhance sample homogeneity and minimize weak agglomerates, the diluted suspension was treated for two minutes at a frequency of 40 kHz and a nominal power of 100 W using an external ultrasonic bath. Subsequently, the suspension was loaded into the measurement cell, ensuring no air bubbles formed and the particle size distribution was calculated based on volume.

Morphology observation

Field emission scanning electron microscopy (FESEM; FEI Quanta FEG 650, USA) was used to analyze the shape and surface properties of the SeNPs. Prior to analysis, dry SeNP powder was sputter-coated onto an aluminum stub using a QUORUM Q150R Plus coating instrument. The shape, size distribution, and aggregation characteristics of the nanoparticles were evaluated via FESEM observation at 100,000× magnification at the Integrated Research Laboratory of Universitas Brawijaya (LRT-UB). Particle size estimation was performed using representative FESEM micrographs.

Energy dispersive X-ray spectroscopy (EDS)

Using an energy-dispersive X-ray spectroscopy (EDS) detector (X-act, Oxford Instruments, UK) integrated with the FESEM, the elemental composition of the produced SeNPs was assessed during FESEM observation. Aztec One software was used for spectrum acquisition and elemental analysis during the EDS study under high-vacuum conditions with an accelerating voltage of 20 kV.

Crystalline analysis

The crystal structure of the synthesized SeNPs was analyzed using an X-ray diffractometer (PANalytical X'Pert3 Powder, Netherlands). The dry SeNP powder was evenly placed on a sample holder with an analysis area of approximately 10 × 10 mm^2. The XRD pattern was recorded using CuKα radiation (λ = 1.542 Å) at 40 kV and 30 mA over a diffraction angle range of 5–50° (2θ), with an angular accuracy of 0.001°.

To determine crystalline selenium phases and assess crystallite properties at various synthesis temperatures, the diffraction patterns were examined. The Debye-Scherrer equation (1) [21], was used to get the mean crystallite size (L), and the Segal formula [Eq. (2)] [22]:

$$L = \frac{K\lambda}{\beta \cos\theta} \quad (1)$$

where L is the average crystallite size, K is the Scherrer constant (0.89), λ is the X-ray wavelength, β is the diffraction peak's full width at half maximum (FWHM) in radians, and θ is the Bragg diffraction angle. The ratio of integrated crystalline peak areas to the entire diffracted area, which includes contributions from crystalline reflections and amorphous backgrounds, was used to compute the crystallinity index (CI).

$$CI = \frac{\Sigma \text{ Area Crystalline Peaks}}{\Sigma \text{ Area Crystalline Peaks} + \text{Area Amorphous}} X\,100\% \quad (2)$$

Applied Science and Engineering Progress, Vol. 20, No. 4, 2027, 8321

2.2.6 Toxicity assessment and fluorescence-associated distribution analysis of SeNPs in Brachionus plicatilis

Brachionus plicatilis from BPBAP Situbondo, Indonesia, was used to evaluate the acute toxicity of SeNPs. In saltwater (32 ppt, pH 7.5, 28 °C) with aeration and Nannochloropsis sp. as feed, rotifers were acclimated for 48 hours. Using 30 rotifers in 25 mL SeNP solutions (0.5-4 mg L^{-1}) with three replicates per concentration, toxicity tests were carried out under static, non-feeding circumstances. The positive control was sodium hypochlorite (150 mg L^{-1}), while the negative control was sterilized seawater. Abbott's formula was used to correct mortality at 24 and 48 hours, and $\log_2$ transformed concentrations were used in probit regression to estimate LC_{20} values with 95% confidence intervals. Additionally, a binomial GLM with a logit link in R was used to evaluate mortality responses (p-value < 0.05) [17].

CLSM was used to analyze the distribution of SeNPs associated fluorescence in *B. plicatilis* following enrichment with Rhodamine B labeled SeNPs. An Olympus IX81 microscope fitted with an Olympus Fluoview FV1000 confocal system was used to wash the rotifers prior to imaging. Olympus FV1000 system with 560-600 nm emission and 543 nm excitation, using the same acquisition parameters. Controls included untreated rotifers, unlabeled rotifers subjected to SeNP, and free rotifers exposed to Rhodamine B. SeNPs associated fluorescence distribution was deduced from fluorescence patterns.

3 Results and Discussion

3.1 *Potential metabolite profiling of gracilaria vermiculophylla byproduct extract and its potential role in SeNP production*

To describe the metabolite composition of the G. vermiculophylla byproduct extract and find substances that might be connected to the production of phytogenic SeNPs, LC-HRMS profiling was used. The promise of this underutilized biomass as a source of chemically diverse chemicals for the synthesis of green nanomaterials was supported by the total ion chromatogram (TIC), which showed a complex metabolite profile (Figure 1). Numerous metabolite classes, such as phenolic related chemicals, nitrogen containing metabolites, terpenoid, and steroid like metabolites, were discovered by accurate mass based annotation (Table 1).

The current study emphasizes the potential use of seaweed-processing leftovers as a chemically varied biomolecular resource for SeNP synthesis in contrast to traditional green synthesis methodologies based on fresh biomass or purified chemicals. A favorable chemical environment for the production of nanoparticles and surface-associated interactions may be created by such complexity [23]. Using extracted ion chromatograms (EIC), the presence and distribution of typical metabolites, such as agmatine Figure 2(a), 4-hydroxybenzaldehyde Figure 2(b), (+)-ar-turmerone Figure 2(c), and β-estradiol Figure 2(d), were further assessed (Figure 2). Nevertheless, the

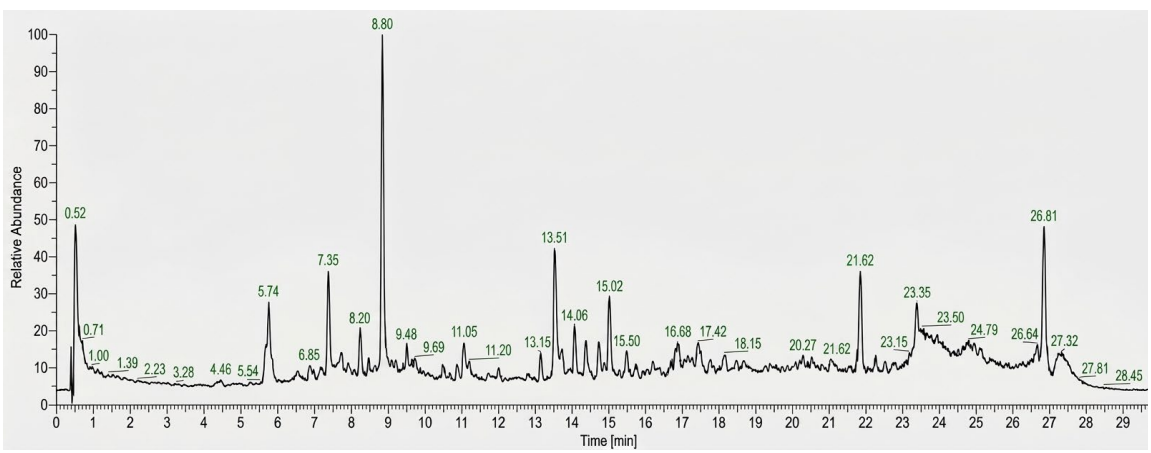

Figure 1: Total ion chromatogram of *G. vermiculophylla* extract.

Table 1: LC-HRMS based putative annotation of metabolites detected in *G. vermiculophylla* by-product extract.

Groups	Compounds	Formula	Annot. Delta Mass [ppm]	Calc. MW	m/z	RT [min]	Area (Max.)
Phenolic	4-Hydroxybenzaldehyde	$C_7H_6O_2$	-2.72	122.0364	123.0437	4.561	6.05E+07
	5-hydroxy-4-methoxy-5,6-dihydro-2H-pyran-2-one	$C_6H_8O_4$	-3.75	144.0417	127.0385	0.874	1.64E+08
Alkaloid/ Nitrogenous compounds	Agmatine	$C_5H_{14}N_4$	-4.48	130.1212	131.1285	0.687	1.33E+08
	5′-S-Methyl-5′-thioadenosine	$C_{11}H_{15}N_5O_3S$	-3.71	297.0884	298.0957	2.440	4.30E+07
	D-(+)-Pipecolinic acid	$C_6H_{11}NO_2$	-4.66	129.0783	130.0856	0.730	7.58E+07
Steroid	β-Estradiol	$C_{18}H_{24}O_2$	-4.94	272.1762	273.1836	10.730	5.66E+06
	Cholecalciferol	$C_{27}H_{44}O$	-4.92	384.3373	385.3445	24.540	6.04E+07
Terpenoid	(-)-ar-Turmerone	$C_{15}H_{20}O$	-4.68	216.1504	217.1590	11.500	4.00E+07
	Muscone	$C_{16}H_{30}O$	-4.92	238.2284	239.2357	22.014	4.58E+07

precise role of each metabolite in selenium transformation or nanoparticle stability cannot be ascertained by LC-HRMS profiling alone. Therefore, complementary physicochemical characterization, such as FTIR, FESEM, EDS, PSA, and XRD analyzes, was used to interpret the possible participation of extract-derived biomolecules.

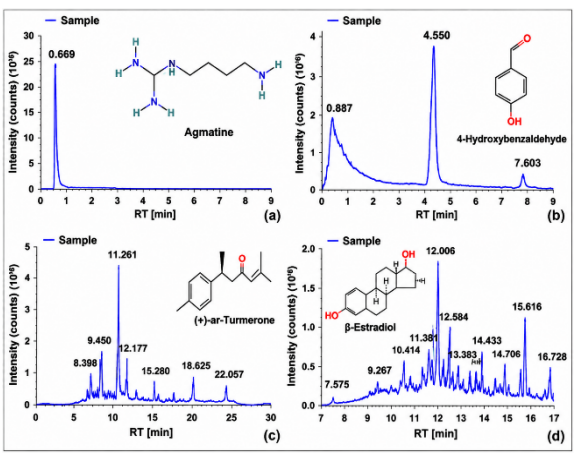

Figure 2: LC-HRMS chromatograms and chemical structures of four standard compounds: (a) Agmatine, (b) 4-Hydroxybenzaldehyde, (c) (+)-ar-Turmerone, and (d) β-Estradiol. Retention times (RT in minutes) are labeled at the corresponding major peaks.

3. 2 *Temperature Related Phytogenic Selenium Nanoparticle Formation*

The color change from greenish-brown to brick-red upon reaction with sodium selenite shows that the synthesis temperature had an impact on the generation of SeNPs utilizing *G. vermiculophylla* byproduct extract. The optical properties of the produced SeNPs changed with temperature, according to UV-Vis spectroscopy (Figure 3).

SeNPs produced at 30°C Figure 3(a) showed a relatively defined absorption maximum at about 320 nm, and all samples displayed absorption features within the wavelength range typically described for biogenic selenium nanostructures. Spectral widening, peak position, and absorption intensity all changed as the synthesis temperature rose. With increased intensity, the absorption maximum moved slightly to about 322 nm at 35°C Figure 3(b), indicating modifications in the behavior of nanoparticle production during synthesis. The absorption maxima further shifted to about 329 nm at 45°C Figure 3(c), along with broader spectral features, indicating possible decreased colloidal stability and increased particle development. UV-Vis spectroscopy was used to assess the temperature-dependent optical characteristics of SeNPs. Within the wavelength range typically observed for biogenic selenium nanostructures, all manufactured samples showed distinctive absorption bands (Figure 4).

Figure 3: *G. vermiculophylla* byproduct extract forms phytogenic selenium nanoparticles (SeNP) at three distinct synthesis temperatures: (a) 30 °C, (b) 35 °C, and (c) 45 °C. The production of SeNP is indicated by the emergence of a reddish colloidal solution.

Applied Science and Engineering Progress, Vol. 20, No. 4, 2027, 8321

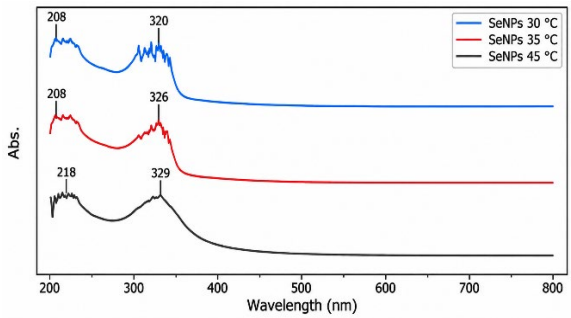

Figure 4: UV-vis spectrum analysis of SeNPs using *G. vermiculophylla* extract at 30˚C, 35˚C, and 45˚C.

The temperature dependent optical changes show that the synthesis temperature affected the aggregation tendency and particle development of SeNPs. While higher synthesis temperatures were linked to greater particle heterogeneity, the comparatively defined spectrum profile at 30°C was consistent with the smaller particle size distribution and decreased apparent agglomeration propensity shown from PSA and FESEM analyzes [7], [11].

The equilibrium between selenium precursor reactivity, particle nucleation, and interactions between evolving selenium structures and extract-derived proteins could be the cause of these variations. While high temperatures may accelerate particle development and collision frequency, encouraging aggregation, moderate temperature settings may favor the production of relatively smaller and more homogeneous nanoparticles. All of these results suggest that the physicochemical evolution of phytogenic SeNPs produced from *G. vermiculophylla* byproduct extract was impacted by synthesis temperature.

3.3 *Integrated physicochemical characterization of SeNPs*

3.3.1 Functional group characteristics and biomolecular association

FTIR analysis was conducted to evaluate functional groups associated with phytogenic SeNPs synthesized using *G. vermiculophylla* byproduct extract and to assess surface-associated biomolecules within the nanoparticle fraction (Figure 5).

FTIR analysis was conducted to characterize functional groups present in the SeNP fraction and to evaluate the association of extract-derived biomolecules after phytogenic synthesis. The FTIR spectrum showed characteristic bands at approximately 3339-3349, 1642, 870, 704, and 600 cm^{-1} (Table 2).

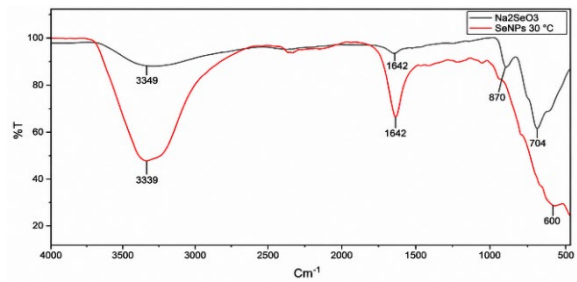

Figure 5: Comparison of FTIR spectra of Na_2SeO_3 and SeNPs synthesized at 30°C. The main absorption peaks were observed at wavenumbers 3339 cm^{-1}, 1642 cm^{-1}, and 600 cm^{-1} for SeNPs.

Table 2: FTIR assigned functional groups associated with biogenic SeNPs.

Wavenumber (cm^{-1})	Assignment	Putative ligand class
3349-3339	O-H stretching	Polyphenols, alcohols, polysaccharides, proteins/peptides
1642	C=O stretching, amide I, C=C aromatic, or H-O-H bending	Proteins, peptides, phenolics, conjugated carbonyl compounds
870	Se-O stretching of selenite	Inorganic selenium precursor, Na_2SeO_3
704	Se-O bending/stretching of selenite	Inorganic selenium precursor, Na_2SeO_3
600	Low-frequency Se-related vibration; residual Se-O, Se-Se, or Se biomolecule interaction	SeNPs surface complex; putative Se biomolecule interaction

The spectrum showed characteristic bands at 3339-3349 cm^{-1} and 1642 cm^{-1}, corresponding to O-H stretching and C=O amide related vibrations, respectively, indicating the presence of oxygen and nitrogen containing organic compounds. Additional bands at approximately 870 and 704 cm^{-1} may represent selenium related vibrations or interactions between selenium containing species and residual organic compounds. The detected hydroxyl, carbonyl, and amine-related functional groups were consistent with the oxygenated and nitrogen-containing metabolites identified by LC-HRMS, indicating that extract derived biomolecules remained associated with the SeNP fraction after synthesis. These functional groups may affect dispersion behavior and contribute to surface interactions of nanoparticles [9]. Nevertheless, individual reducing agents, capping

compounds, or reaction processes cannot be explicitly confirmed by FTIR analysis alone, nor can it identify particular molecules. These results are regarded as evidence of biomolecular connection and surface interaction [8], [24].

3.3.2 Morphology and particle size distribution of SeNPs

The temperature at which SeNPs were synthesized affected their shape and particle size distribution. SeNPs produced at 30 °C Figure 6(a) had a comparatively spherical shape and less obvious aggregation than those produced at higher temperatures, according to FESEM analysis (Figure 6). Particle morphology was observed by FESEM, and particle size distribution was determined by PSA. PSA analysis further showed an average particle size of approximately 50 nm at 30 °C, whereas samples synthesized at 35 °C Figure 6(b) and 45 °C Figure 6(c) exhibited broader size distributions with a shift toward larger particle populations. These changes were accompanied by broader UV-Vis absorption profiles at higher synthesis temperatures, suggesting greater particle heterogeneity. Overall, the results indicate temperature-dependent differences in particle growth and aggregation behavior.

The smaller particle size observed at 30 °C may reflect more favorable interactions between selenium species and extract derived biomolecules during nanoparticle formation [25]. FTIR analysis indicated functional groups potentially associated with biomolecules involved in SeNP formation and surface stabilization, while LC-HRMS revealed several metabolite classes in the *G. vermiculophylla* byproduct extract. However, these analyses do not establish the direct molecular mechanisms of nanoparticle stabilization. Collectively, the characterization results suggest that extract composition and synthesis temperature were associated with the observed differences in SeNP morphology and particle size distribution.

3.4 *Elemental Composition and Crystalline Characteristics of SeNPs*

3.4.1 Elemental confirmation by EDS analysis

Energy dispersive X-ray spectroscopy (EDS) was performed to evaluate the elemental composition of SeNPs synthesized using *G. vermiculophylla* by-product extract under different synthesis temperatures (Figure 7). Selenium was detected as the dominant element in all analyzed nanoparticle regions, with a characteristic selenium signal observed at approximately 1.4 keV. The selenium composition varied among synthesis conditions, ranging from 22.96% to 78.15% (atomic composition), with the highest selenium proportion detected in SeNPs synthesized at 30°C Figure 7(a), followed by 35°C Figure 7(b) and 45°C Figure 7(c). The variation in selenium composition indicates that synthesis temperature influenced the elemental characteristics of the resulting nanoparticle fraction [11], [15]. However, EDS analysis provides elemental composition information only and cannot determine selenium oxidation states or directly confirm the conversion of Se^{4+} to elemental selenium (Se^0). Therefore, the formation of selenium nanostructures was interpreted based on the combined evidence obtained from UV–Vis spectroscopy, FTIR, and XRD analyses rather than EDS data alone.

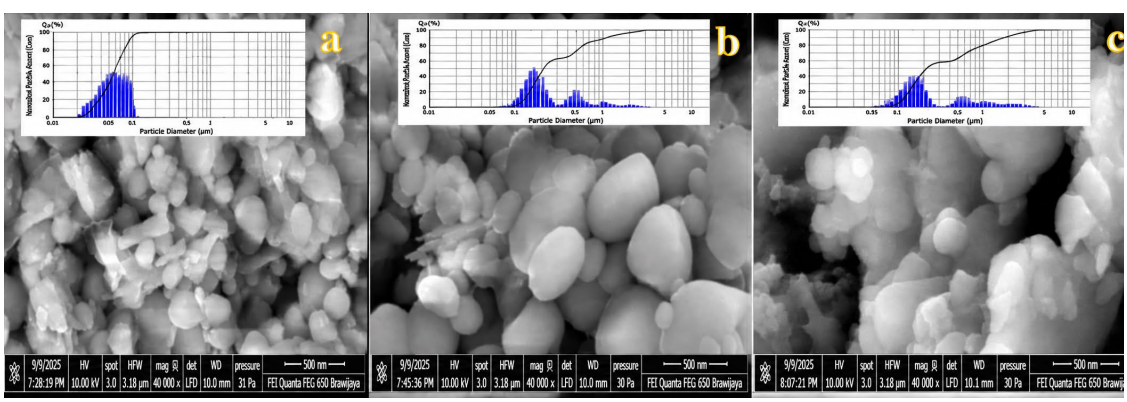

Figure 6: FESEM images and particle size distribution of phytogenic selenium nanoparticles (SeNPs) synthesized at different temperatures: (a) 30 °C, (b) 35 °C, and (c) 45 °C. Insets show the cumulative particle size distribution (Q_3, %) profiles. Scale bars represent 500 nm.

Applied Science and Engineering Progress, Vol. 20, No. 4, 2027, 8321

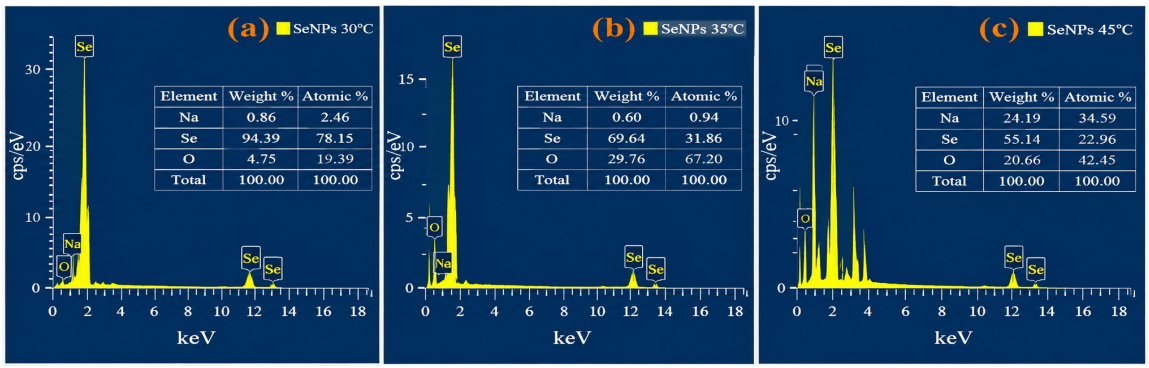

Figure 7: EDS element maps for synthesized samples demonstrate the findings of the EDS investigation of nanoparticle synthesis and the dominance of Se: (a). SeNPs 30°C (b). SeNPs 35°C, (c). SeNPs 45°C.

In SeNPs made at 30°C and 35°C, sodium was found as a small elemental component (0.60–0.86 wt%). On the other hand, samples synthesized at 45°C showed a smaller contribution of selenium (55.14%) and a higher quantity of sodium (24.19 weight percent). This discrepancy probably results from differences in the nanoparticle fraction's elemental makeup under various production conditions [15]. Reaction temperature affects the creation of nanoparticles, as evidenced by the reported elemental variances across the different synthesis temperatures and the variations in particle properties found by FESEM and PSA analyzes. Further research utilizing complementary methods like XPS is necessary to understand elemental composition, particle development, and surface chemistry. EDS analysis shows that synthesis temperature affects the elemental makeup of the final nanoparticle fraction and offers elemental evidence of selenium incorporation into the produced nanoparticles.

3.4.2 Crystalline analysis

The crystalline structure and phase composition of phytogenic SeNPs made using *G. vermiculophylla* byproduct extract were assessed by XRD analysis. The diffraction patterns of SeNPs synthesized at 30, 35, and 45°C showed characteristic reflections at approximately 2θ = 23.5°, 29.7°, 41.3°, 43.7°, 45.4°, and 51.7°. According to JCPDS references (No. 01-086-2246, 01-086-2244, and 00-006-0362), the diffraction pattern was compatible with hexagonal selenium phases, and the main peak at 29.7° matched the (101) crystallographic plane of selenium. No discernible secondary crystalline phases were found within the XRD detection limit, according to the lack of additional significant peaks (Figure 8).

Crystallite size was estimated using the Debye-Scherrer equation based on the (101) diffraction peak. The calculated crystallite domains increased with synthesis temperature, with approximate values of 20, 30, and 55 nm for SeNPs synthesized at 30, 35, and 45°C, respectively. This increase points to better crystal formation at higher temperatures. These figures, which represent crystallite domains rather than precise nanoparticle sizes, can account for the differences in crystallite size as reported by XRD and particle size as determined by PSA and FESEM [25]. The smaller crystallite size at 30°C was consistent with the narrower UV-Vis spectral profile, lower aggregation tendency, and smaller particle distribution observed in previous analyzes. These findings imply that synthesis temperature affects the structural characteristics of phytogenic SeNPs and the formation of selenium crystals.

3.5 *Acute toxicity and fluorescence-related distribution of se nanoparticles in brachionus plicatilis*

Brachionus plicatilis is a suitable marine ecotoxicological model due to its small body size, short life cycle, ecological relevance, and sensitivity to environmental contaminants, including engineered nanoparticles. Previous studies using ZnO and AgNP nanoparticles have demonstrated the applicability of rotifers for nanoparticle toxicity assessment; however, differences in nanoparticle composition, physicochemical properties, and exposure conditions require these studies to be considered as methodological references rather than direct comparisons of SeNPs toxicity [16], [26]. Exposure of *B. plicatilis* to phytogenic SeNPs resulted in a concentration- and time-dependent mortality pattern (Figure 9).

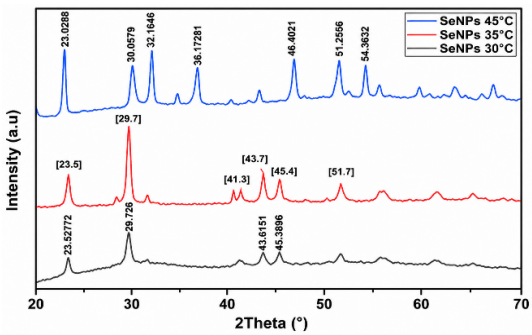

Figure 8: XRD patterns of samples synthesized at 30°C, 35°C, and 45°C; variations in peak intensity and sharpness indicate temperature dependent changes in SeNP crystallinity.

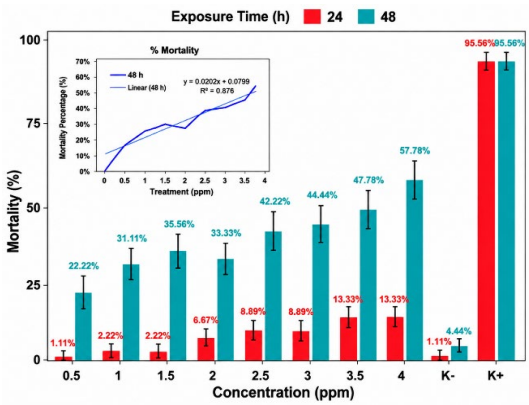

Figure 9: Analysis of the effect of concentration and exposure time on the percentage of mortality of test objects.

Brachionus plicatilis is a suitable marine ecotoxicological model because of its short life cycle, ecological relevance, and sensitivity to environmental contaminants, including engineered nanoparticles [16]. In the present study, mortality increased with exposure duration, from 1.11-13.33% after 24 h to 22.22-57.78% after 48 h across 0.5-4.0 mg L^{-1} SeNPs. While the positive control generated roughly 95.56% mortality, indicating sufficient assay performance, the negative control mortality stayed low. Probit regression estimated a 48 h LC_{50} of 3.76 mg L^{-1} (95% CI: 3.08-4.44 mg L^{-1}).

The synthesized SeNP formulation and experimental circumstances should be taken into consideration when interpreting this LC_{50}. Particle composition, size, aggregation, surface characteristics, colloidal stability, exposure time, and organism-specific sensitivity all affect nanoparticle toxicity [27]. Therefore, toxicity values reported for other nanoparticle systems or selenium forms should be considered contextual rather than direct benchmarks. Although SeNP-enriched rotifers have been investigated for nutritional applications in aquaculture [28], quantitative information on acute SeNP toxicity in *B. plicatilis* remains limited. CLSM revealed SeNP-associated fluorescence predominantly within internal body regions, particularly near the digestive tract, consistent with the particle feeding behavior of rotifers (Figure 10).

Previous fluorescence based studies have similarly detected nanoscale suspended particles within the digestive tract of *B. plicatilis* [29]. These observations confirm the localization of selenium driven by the feeding process. These findings provide preliminary data on acute toxicity and evidence of localization to support the determination of exposure ranges for future SeNP enrichment studies utilizing marine live feed organisms. Integrating toxicity assessment with fluorescence based localization provides biosafety information for evaluating phytogenic SeNPs as candidates for a sustainable selenium supply. This study establishes a preliminary framework linking the utilization of seaweed by-products, green nanotechnology, and rotifer-based safety assessment to support the development of future selenium enrichment strategies for marine aquaculture live feed systems [30].

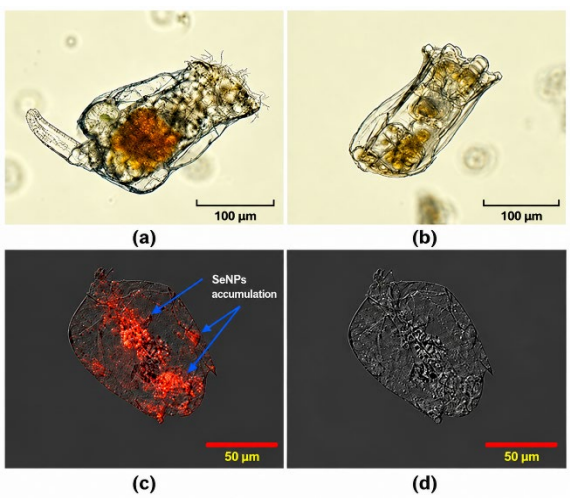

Figure 10: Flourescence associated distribution of SeNPs in *Brachionus plicatilis*. (a-b) Light microscopy images showing rotifer morphology in internal regions. (c) CLSM image showing SeNP associated fluorescence signals in internal body regions. (d) Corresponding bright field CLSM image without fluorescence signal. Scale bars: 100 µm (a-b) and 50 µm (c-d).

Applied Science and Engineering Progress, Vol. 20, No. 4, 2027, 8321

4 Conclusions

This study demonstrates the potential of *G. vermiculophylla* processing by-products as a sustainable biomolecular resource for phytogenic SeNPs synthesis. Seaweed-derived biomolecules supply components linked to SeNPs production and surface contacts, while synthesis temperature affects nanoparticle properties, according to the combination of metabolite profiling and physicochemical characterization. Among the tested conditions, SeNPs synthesized at 30°C exhibited the most favorable physicochemical profile, with relatively smaller particle size, spherical morphology, lower aggregation observed by FESEM analysis, and crystalline selenium characteristics. Acute toxicity evaluation using *B. plicatilis* revealed concentration and exposure duration dependent responses, with a 48 h LC_{50} value of 3.76 mg L^{-1} SeNPs. Fluorescence associated localization indicated that SeNPs associated signals mainly in internal body regions, particularly the digestive tract, providing preliminary insight into nanoparticle–rotifer interactions.

Acknowledgments

The Marine and Fisheries Education Center, Marine and Fisheries Polytechnic, Karawang, Ministry of Marine Affairs and Fisheries, Indonesia.

Authors contribution

D.W.: conceptualization, methodology, investigation, data curation, data analysis, writing an original draft, editing, validation; U.Y.: conceptualization, writing, review, editing, validation, resources, methodology, investigation; A.K.: writing, review, editing, Visualization, Resources, Methodology, Investigation; A.R.F.: writing, review & editing, Resources, Methodology, Investigation; H.S.: writing, review & editing, Visualization, Methodology, Investigation; N.R.C.: investigation, reviewing, and editing, project administration; D.R.M.: review, editing, project administration. All Authors have read and agreed to the published version of the manuscript.

Conflicts of Interest

The authors declare no conflict of interest.

Declaration of Generative AI and AI-assisted Technologies in the Writing Process

The authors used the ChatGPT tool to enhance the language and readability of the manuscript.

References

[1] M. Fadhlullah, S. B. Prasetyati, I. Pudoli, and C. Lo, "Preliminary economic potential evaluation of seaweed Gracilaria sp. biomass waste as bioindustry feedstock through a biorefinery approach: a case study in Karawang, Indonesia," *3BIO: Journal of Biological Science*, vol. 4, no. 1, pp. 42–53, Apr. 2022, doi: 10.5614/3bio.2022.4.1.6.

[2] Food and Agriculture Organization of the United Nations, *The State of World Fisheries and Aquaculture 2004*. Rome, Italy: Food and Agriculture Organization of the United Nations, 2004.

[3] R. Araújo et al., "Current status of the algae production industry in Europe: an emerging sector of the blue bioeconomy," *Frontiers in Marine Science*, vol. 7, Art. no. 626389, Jan. 2021, doi: 10.3389/fmars.2020.626389.

[4] M. A. O. Dawood et al., "Selenium nanoparticles as a natural antioxidant and metabolic regulator in aquaculture: A review," *Antioxidants*, vol. 10, no. 9, Art. no. 1364, Aug. 2021, doi: 10.3390/antiox10091364.

[5] R. Salvador, F. N. Puglieri, A. Halog, F. G. de Andrade, C. M. Piekarski, and A. C. De Francisco, "Key aspects for designing business models for a circular bioeconomy," *Journal of Cleaner Production*, vol. 278, Art. no. 124341, Jan. 2021, doi: 10.1016/j.jclepro.2020.124341.

[6] N. Kumar, K. K. Krishnani, and N. P. Singh, "Comparative study of selenium and selenium nanoparticles with reference to acute toxicity, biochemical attributes, and histopathological response in fish," *Environmental Science and Pollution Research*, vol. 25, no. 9, pp. 8914–8927, Mar. 2018, doi: 10.1007/s11356-017-1165-x.

[7] E. O. Mikhailova, "Selenium nanoparticles: Green synthesis and biomedical application," *Molecules*, vol. 28, no. 24, Art. no. 8125, Dec. 2023, doi: 10.3390/molecules28248125.

[8] M. T. El-Saadony et al., "Selenium nanoparticles: Eco-friendly synthesis, biological activities and

biomedical applications - A comprehensive review," *Materials Today Bio*, vol. 37, Art. no. 102946, Apr. 2026, doi: 10.1016/j.mtbio.2026.102946.

[9] U. Farooq and A. Kusar, "Green synthesis of selenium nanoparticles for enhanced photocatalysis applications," *Discover Chemistry*, vol. 3, no. 1, Art. no. 287, May 2026, doi: 10.1007/s44371-026-00741-2.

[10] J.-S. Kim, C. Choi, and H.-H. Lee, "Changes in the biological activities of *Gracilaria verrucosa* extracted using different extraction solvents," *Applied Sciences*, vol. 13, no. 22, Art. no. 12314, Nov. 2023, doi: 10.3390/app132212314.

[11] A. Sentkowska, J. Konarska, J. Szmytke, and A. Grudniak, "Herbal polyphenols as selenium reducers in the green synthesis of selenium nanoparticles: Antibacterial and antioxidant capabilities of the obtained SeNPs," *Molecules*, vol. 29, no. 8, Art. no. 1686, Apr. 2024, doi: 10.3390/molecules29081686.

[12] H.-J. Kim et al., "Feeding effect of selenium enriched rotifers on larval growth and development in red sea bream Pagrus major," *Aquaculture*, vol. 432, pp. 273–277, Aug. 2014, doi: org/10.1016/j.aquaculture.2014.05.021.

[13] M. Ponce et al., "Toxicity and biochemical transformation of selenium species in rotifer (*Brachionus plicatilis*) enrichments," *Aquaculture*, vol. 484, pp. 105–111, Feb. 2018, doi: 10.1016/j.aquaculture.2017.10.040.

[14] G. Muthusamy, S. Thangasamy, M. Raja, S. Chinnappan, and S. Kandasamy, "Biosynthesis of silver nanoparticles from *Spirulina* microalgae and its antibacterial activity," *Environmental Science and Pollution Research*, vol. 24, no. 23, pp. 19459–19464, Aug. 2017, doi: 10.1007/s11356-017-9772-0.

[15] D. Sharma, S. Afzal, and N. K. Singh, "Nanopriming with phytosynthesized zinc oxide nanoparticles for promoting germination and starch metabolism in rice seeds," *Journal of Biotechnology*, vol. 336, pp. 64–75, Aug. 2021, doi: 10.1016/j.jbiotec.2021.06.014.

[16] S. Mohammadi, N. Ahmadifard, B. Atashbar, A. Nikoo, and R. Manaffar, "Long-term effect of zinc oxide nanoparticles on population growth, reproductive characteristics and zinc accumulation of marine rotifer, Brachionus plicatilis," *International Journal of Aquatic Biology*, vol. 9, no. 5, pp. 333–343, Oct. 2021, doi: 10.22034/ijab.v9i5.1292.

[17] U. Yanuhar, M. S. Widodo, A. R. Faqih, H. Suryanto, and N. R. Caesar, "Study of the toxicity of Fe3O4 nanoparticles on Pacific white leg shrimp (*Litopenaeus vannamei*) and the antibacterial efficacy against *Vibrio harveyi*," *Journal of Hazardous Materials Advances*, vol. 18, Art. no. 100674, May 2025, doi: 10.1016/j.hazadv.2025.100674.

[18] J. Yu et al., "Effects of nanoplastics exposure on ingestion, life history traits, and dimethyl sulfide production in rotifer *Brachionus plicatilis.*," *Environmental Pollution*, vol. 344, Art. no. 123308, Mar. 2024, doi: 10.1016/j.envpol.2024.123308.

[19] Reetu, M. Mukherjee, and M. P. Rai, "Bioinspired green synthesis of nanomaterials from algae," *Bioinspired and Green Synthesis of Nanostructures*, pp. 141–156, 2023, doi: 10.1002/9781394174928.ch6.

[20] A. Behera, M. K. D. Jothinathan, S. Saravanan, S. T. Selvan, R. R. Renuka, and G. P. Srinivasan, "Green synthesis of selenium nanoparticles from clove and their toxicity effect and anti-angiogenic, antibacterial and antioxidant potential," *Cureus*, vol. 16, no. 3, Art. no. e55605, Mar. 2024, doi: 10.7759/cureus.55605.

[21] N. S. Murthy, S. T. Correale, and H. Minor, "Structure of the amorphous phase in crystallizable polymers: poly (ethylene terephthalate)," *Macromolecules*, vol. 24, no. 5, pp. 1185–1189, Mar. 1991, doi: 10.1021/ma00005a033.

[22] M. Kawsar, M. S. Hossain, N. M. Bahadur, and S. Ahmed, "Synthesis of nano-crystallite hydroxyapatites in different media and a comparative study for estimation of crystallite size using Scherrer method, Halder-Wagner method size-strain plot, and Williamson-Hall model," *Heliyon*, vol. 10, no. 3, Art. no. e25347, Feb. 2024, doi: 10.1016/j.heliyon.2024.e25347.

[23] A. D. Harfiyani et al., "LC-HRMS-Based Metabolomic Profiling and Antioxidant Activity of Sargassum ilicifolium Under Different Pretreatments, Extraction Methods, and Solvents," *Antioxidants*, vol. 15, no. 4, Art. no. 433, Mar. 2026, doi: 10.3390/antiox15040433.

[24] K. Pyrzynska and A. Sentkowska, "Biosynthesis of selenium nanoparticles using plant extracts," *Journal of Nanostructure in Chemistry*, vol. 12, pp. 467-480, Aug. 2022, doi: 10.1007/s40097-021-00435-4.

[25] H. M. M. Ibrahim, "Green synthesis and

Applied Science and Engineering Progress, Vol. 20, No. 4, 2027, 8321

characterization of silver nanoparticles using banana peel extract and their antimicrobial activity against representative microorganisms," *Journal of Radiation Research and Applied Sciences*, vol. 8, no. 3, pp. 265–275, Jul. 2015, doi: 10.1016/j.jrras.2015.01.007.

[26] T. O. Garcia et al., "In vivo toxicity of silver nanoparticles in the marine rotifer *Brachionus plicatilis*: Integrating metabolic activity and generation of reactive oxygen species," *Coatings*, vol. 16, no. 2, Art. no. 152, Jan. 2026, doi: 10.3390/coatings16020152.

[27] R. Abbasi, G. Shineh, M. Mobaraki, S. Doughty, and L. Tayebi, "Structural parameters of nanoparticles affecting their toxicity for biomedical applications: a review," *Journal of Nanoparticle Research*, vol. 25, Art. no. 43, Feb. 2023, doi: 10.1007/s11051-023-05690-w.

[28] S. Ghaderpour, N. Ahmadifard, N. Agh, A. Estévez, and Z. Vahabzadeh, "Short-term enrichment of microalgae with inorganic selenium and zinc and their effects on the mineral composition of microalgae and marine rotifer *Brachionus plicatilis*," *Aquaculture Nutrition*, vol. 27, no. 6, pp. 2772-2785, Dec. 2021, doi: 10.1111/anu.13406.

[29] T. Gomes et al., "Ecotoxicological impacts of micro-and nanoplastics in terrestrial and aquatic environments," in *Microplastic in the Environment: Pattern and Process*, M. S. Bank, Ed. Cham, Switzerland: Springer, 2022, pp. 199–260, doi: 10.1007/978-3-030-78627-4_7.

[30] P. V Nagime et al., "Biogenic selenium nanoparticles: a comprehensive update on the multifaceted application, stability, biocompatibility, risk, and opportunity," *Zeitschrift für Naturforschung C*, vol. 80, no. 11–12, pp. 627–655, 2025, doi: 10.1515/znc-2024-0176.

.